Review

Fabrication of MAX-Phase-Based Ceramics by Three-Dimensional Printing

Y. Ma[1], X. Yin[*1], X. Fan[1], N. Travitzky[2], P. Greil[2]

[1]Science and Technology on Thermostructural Composite Materials Laboratory,
Northwestern Polytechnical University, Xi¡¯an, Shaanxi, 710072, PR China
[2]Department of Materials Science (Glass and Ceramics),
University of Erlangen-Nuremberg, Erlangen, Germany.

Abstract

Three-dimensional printing (3DP) is a flexible and cost-effective method for direct digital manufacturing that provides capabilities for creating a wide range of part geometries in a broad variety of materials. Recently, a combined process of 3DP and reactive melt infiltration (RMI) has been applied to fabricate MAX-phase-based ceramics, exhibiting great potential in the fabrication of bulk compounds with complicated shape. This paper briefly summarizes the fabrication of Ti_3AlC_2- and Ti_3SiC_2-based ceramics with the combined process. 3DP facilitates the prior design of a porous preform with specific pore distribution and microstructure, which is beneficial to the control of the volume change of the following reaction in the RMI process, promoting the near-net-shape fabrication of MAX-phase-based ceramics with high flexibility in component geometry.

Keywords: Three-dimensional printing, RMI, Ti_3SiC_2, Ti_3AlC_2.

I. Introduction

MAX phases are thermodynamically stable nanolaminates exhibiting unusual and unique properties. They have combined characteristics of metal and ceramics [1–3] and exhibit attractive properties such as good oxidation resistance, low density, high modulus, good thermal and electrical conductivity, excellent thermal shock resistance and high-temperature strength, and easy machinability [4–6]. They are considered promising structural/functional materials for high-temperature applications [7–9]. MAX phases have also been successfully used as reinforcement to improve the mechanical properties of intermetallic and ceramic-based composites [10].

Recently, several methods, such as chemical vapor deposition (CVD) [11,12], mechanical alloying (MA) [13,14], self-propagating high-temperature synthesis (SHS) [15–17], hot pressing (HP) [18] and spark plasma sintering (SPS) [13], have been applied to fabricate MAX-phase-based materials and the properties of these materials studied extensively.

Tzenov *et al.* [19] fabricated dense Ti_3AlC_2 bulk materials by means of reactive hot isostatic pressing (HIP) of a Ti, C, and Al_4C_3 powder mixture at 70 MPa, 1400 °C for 16 h. Yeh *et al.* [17] used a $3Ti/1.25C/0.25Al_4C_3$ mixture as the starting powder to fabricate Ti_3AlC_2 ceramics by means of SHS, and the increase of the preform density prior to the SHS process led to the increase of Ti_3AlC_2 content from 50.5 to 73.2 wt%. Yanga *et al.* [13] combined MA and SPS methods for the fabrication of Ti_3AlC_2-based material.

Dense Ti_3AlC_2 was fabricated by means of SPS at 1050 °C for 10 ~ 20 min with mechanically alloyed powders from a starting mixture of 3Ti/1.1Al/2C. Han *et al.* [20] fabricated polycrystalline bulk Ti_3AlC_2 with HP from a mixture of TiC_x (x = 0.6) and Al powder under 25 MPa pressure in the temperature range of 800 to 1600 °C, fully dense and pure Ti_3AlC_2 was synthesized by means of HP above 1400 °C; Vickers hardness up to 6 GPa and flexural strength higher than 900 MPa were measured for the as-fabricated bulk Ti_3AlC_2 samples.

CVD was the early method for the fabrication of dense Ti_3SiC_2 ceramics with high purity [11]. Deposition is usually conducted at 1300 ~ 1600 °C with $SiCl_4$, $TiCl_4$, CCl_4 and H_2 as source gases. However, CVD could only be used for the fabrication of thin films and coatings composed of MAX phases. Barsoum *et al.* [2] used the HIP method for the fabrication of bulk Ti_3SiC_2 materials. Powder blends of Ti, C and SiC with a molar ratio of 3:2:1 were cold-pressed under 180 MPa. In order to obtain dense materials, the compacted green bodies were then reacted in the HIP device at 1600 °C for 4 h under 40 MPa. Gao *et al.* fabricated dense Ti_3SiC_2 bulk material by means of SPS up to 1300 °C [21]. The composition of starting powder mixture was Ti:Si:TiC = 1:1:2 (molar ratio). The as-fabricated Ti_3SiC_2 material contained only 2 wt% TiC_x impurity. *In-situ* hot pressing was conducted by Zhou *et al.* [3] using mixed powders with a molar ratio of Ti:Si:C = 0.42:0.23:0.35. Ti_3SiC_2 bulk material with purity of 93 wt% was fabricated at 1550 °C in an atmosphere of flowing Ar. Further study [22] shows that using

a small amount of Al to replace the Si atom in Ti_3SiC_2 could help reduce the content of remaining TiC and obtain $Ti_3Si(Al)C_2$ with high purity. The arc-melting and annealing route was applied by Arunajatesan *et al.* for the synthesis of bulk Ti_3SiC_2 from the Ti, Si, and C powders [23]. The bulk sample containing about 2 vol% TiC as the second phase was made from Si-deficient and C-rich starting compositions.

For all these fabrication methods, raw materials with high activity are preferred in order to fabricate dense materials with high purity. The fabrications are always conducted at high temperatures with external force applied for a long reaction time, which restricts the fabrication of bulk samples with complicated shape.

In order to fabricate MAX-phase-based ceramics with complicated shape, Sun *et al.* [24] combined three-dimensional layered printing (3DP), cold isotactic pressing (CIP) and sintering for the fabrication of Ti_3SiC_2-powder-based structures. Three-dimensional Ti_3SiC_2 structures with complex geometry and high density can be fabricated (Fig. 1).
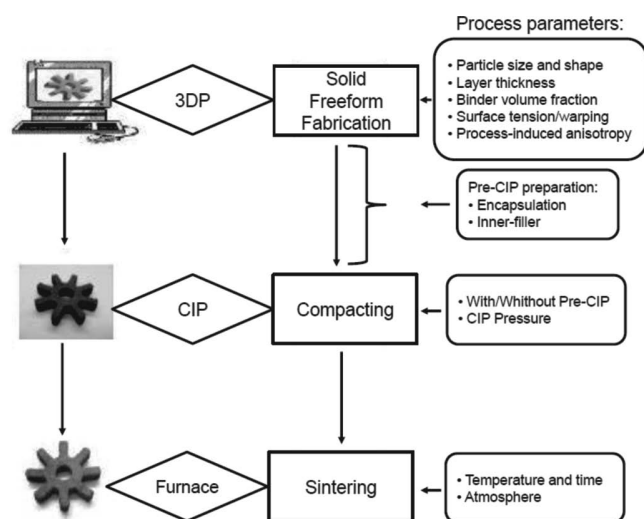

Fig. 1: The three-stage process and the corresponding fabricated parts [24].

3DP allows rapid flexible production of prototype parts directly from a CAD model, with no tooling or geometric limitation [25–27], which is beneficial to efficiently producing accurate parts with complex geometries. Two basic different 3DP approaches can be distinguished, the first one is a direct inkjet printing (DIP) method in which the powder in the form of a colloidal suspension (e.g. ink) passes through the print head to form the free-standing shape [28]; the second one is an indirect method in which the liquid binder is printed onto preplaced powder to join the microparticles together [29]. The DIP method is able to produce dense ceramic bodies without post-processing treatment [30]. Indirect printing has much greater flexibility, but the as-printed ceramic parts always contain a lot of pores, leading to high porosity and low strength. In the work of Sun *et al.* [24], CIP was used for densification, however, the overall shrinkage of the as-fabricated parts was about 25 ~ 30 vol%. Therefore, a geometric compensation factor was incorporated into the design of the CAD model.

A number of studies have used the combination of 3DP and reactive melt infiltration (RMI) to fabricate dense ceramics with near-net shape. In the RMI process, a molten metal spontaneously penetrates into pores driven by capillary force, and then reacts with the porous preform to form the bulk compounds. During RMI, no external pressure is required, which is beneficial to the near-net-shape fabrication of complex structures and offers high flexibility with regard to component geometry [31–33]. The combined process has been successfully applied to fabricate SiSiC with complicated shape. Moon *et al.* [34] firstly used 3DP to prepare porous carbonaceous preforms composed of glassy carbon powders with a particle size of 45 ~ 105 μm, using an acetone-based furfuryl resin binder as a printing solution. After liquid silicon infiltration at 1450 °C in N_2 atmosphere, a SiSiC composite with a coarse SiC grain structure was formed. Travitzky *et al.* [35] prepared a SiC-C preform from a mixture of SiC and starch-cellulose powders by means of 3D printing and pyrolysis, and then dense SiSiC was obtained with the infiltration of liquid silicon into the SiC-C preform [36].

Dense Ti_3AlC_2- and Ti_3SiC_2-based ceramic parts with a complex shape were fabricated with a combined method of RMI and 3DP [10, 37–40]. By means of the pre-design of the preform with 3DP and control of the subsequent reactions, it is possible to control dimensional changes during RMI. The as-fabricated ceramics can attain good mechanical properties. The following paper will focus on progress in the fabrication of Ti_3AlC_2- and Ti_3SiC_2-based ceramics. It consists of three parts: the first part is the structural design of the porous preform, which directly affects the infiltration kinetics of the melt in the RMI process; the second part is the reaction mechanism during the fabrication process; the third part summarizes the microstructure and mechanical properties of different MAX-phase-based ceramics, indicating the relationship between properties and microstructure.

II. Structural Design of the Preform

(1) Infiltration kinetics during the fabrication of max-phase-based ceramics

Metal melt infiltration into a porous solid preform is one of the preferred methods to fabricate ceramic-metal and ceramic matrix composites. A molten metal can penetrate into the pores driven either by an external force (squeeze casting) or by the action of capillary pressure created when the liquid wets the solid [41]. The reaction between the porous ceramic preform and the molten metal may considerably enhance the wettability. Compared to pressure-assisted infiltration techniques such as squeeze casting or gas-pressure infiltration, RMI offers high flexibility with regard to component geometry. With the pre-design of the composition and microstructure of porous preform, bulk materials with complex and near-net shape can be obtained [42, 43].

The infiltration of Al melt into a TiC/TiO_2 preform was initially used to fabricate Ti_3AlC_2-based ceramics with high crack resistance [10, 37, 38]. After that, works on fabricating Ti_3SiC_2-based ceramics by means of LSI were

conducted [41 – 45]. Lu *et al.* [44] fabricated Ti_3SiC_2-based ceramic with the infiltration of silicon melt into a TiC-C preform. Nan *et al.* [39] fabricated Ti_3SiC_2-based ceramics with high electrical conductivity and bending strength in a joint process of three-dimensional printing (3DP) and liquid silicon infiltration. Shan *et al.* [45] synthesized Ti_3SiC_2 bulk ceramics by infiltrating Ti/TiC preform with silicon melt. Hwang *et al.* [46] fabricated high-purity Ti_3SiC_2 compounds with the infiltration of silicon melt into a TiC_x (x = 0.67) preform. Ti_2SnC was also recently fabricated with the infiltration of Sn melt into $TiC_{0.5}$ [47]. Besides the fabrication of bulk compounds, RMI has also been considered as an effective way to introduce Ti_3SiC_2 into fiber-reinforced ceramic matrix composites such as C/C-SiC and C/SiC composites [6, 8, 42, 48] for optimizing mechanical and tribological performance.

During RMI, the wetting behavior of the melt on the pore surface in the preform is the main factor affecting the infiltration kinetic, which determines the microstructure uniformity and the maximum size of the as-fabricated material. Once metal melt penetrates into the preform, a reaction may occur at the metal melt-ceramic interface. In the course of the reaction, the metal firstly diffuses into the formed solid phases, and then reacts with the ceramic particles, and the infiltration process changes from reaction control to diffusion control. Fast infiltration speed is conducive to the homogeneous microstructure of as-fabricated material, and the infiltration kinetics evaluation should always be considered as a primary factor.

The infiltration kinetics of metal melt into the porous preform is provided by Darcy¡s law [49]. Infiltration depth, h, was estimated as a function of time, t. (Eq.1)

$$h= \left[t \left(\frac{\varepsilon_p}{1- \varepsilon_p} \right) \frac{r\lambda\gamma}{6.25\mu}\cos\theta \right]^{1/2} \qquad (1)$$

where ε_p is the pore volume fraction; r is the pore radius; μ denotes the viscosity of melt; λ is the particle size factor; γ is the surface tension and θ is the wetting angle.

During the infiltration process, the pore radius and wetting angle directly affect the infiltration depth in accordance with Eq. (1). Table 1 summarizes the infiltration depth of Al and Si melt into the TiC preform with different pore radius within 60 s at 1000 °C and 1600 °C in vacuum, respectively [10, 40]. For pores with same radius, the infiltration rate of Si melt and Al melt varies slightly, which can be attributed to the close viscosity and wetting angle.

Table 1: Infiltration depth of Al and Si melt into a TiC preform with different pore radius in 60 s at 1000 °C and 1600 °C in a vacuum [10, 40].

Pore radius (µm)	Infiltration depth (cm)	
	Al melt	Si melt
0.07	2	—
1	2.4	2.5
23	14.2	15.2
30	20	—

Infiltration efficiency could be significantly improved with the use of a preform with bimodal pore size distribution [50]. Pores with larger radius are the inter-agglomerate ones, the ones with smaller radius are the intra-agglomerate pores (Fig. 2). The existence of large pores guarantees the rapid infiltration of metal melt.
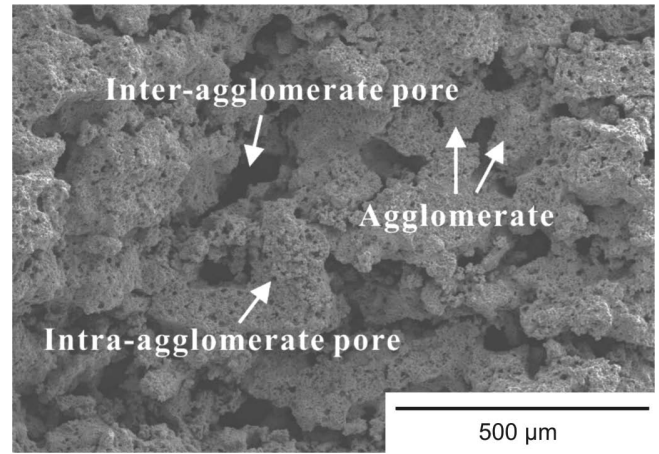

Fig. 2: Typical microstructure of a preform with bimodal pore size distribution [40].

(2) Microstructural design of the preform

In order to obtain a preform with the bimodal pore size distribution mentioned in II(1), an indirect 3DP process was used for the structural design. The basic design principles and essential factors are as follows:

3DP is a layered fabrication process in which the sliced 2D profile of a computer model is printed on a fresh layer of powder via deposition of a suitable binder. Successive 2D profiles are then printed on a freshly laid layer of powder until the entire model is completed. The printed binder joins the respective profiles of each layer together. The part is completed upon removal of the unbound powder and suitable post-processing [51].

Successful realization of a specific 3DP process involves not only the printing process itself, but also the formulation of a suitable combination of a powder and binder material system along with process details for printing and post-processing, both of which play major role in determining the characteristics of the as-produced parts. During the building process, there is no phase change of material involved based on the inkjet principle, guaranteeing its high manufacturing speed.

In order to attain a homogeneous and coherent spreading of each layer during the printing procedure, particle or granulate dimension, morphology and flowability are important factors to be considered. Generally, in order to obtain ideal deposition ability, spherical powder particles with a diameter of 20 µm and larger are preferable [52]. Spherical powders tend to flow better and have low internal friction. Fine powders (~ 1 µm) tend to agglomerate owing to van der Waal's forces and moisture effects, but have the potential advantages of increase sinterability, lower surface roughness, smaller minimum features, and thinner layers [53]. The application of spray-dried [54] or freeze-dried [10, 39] granules enables the use of fine sinter-

ing-active particles. The higher the pourability of powder, the thinner the layers are built by the leveling roller, and hence the higher the quality of the printed body. It was also demonstrated that the wettability and pourability of powders can be sufficiently improved by means of plasma treatment [55].

While 3DP may produce porous preforms with a high degree of freedom in terms of geometry and shape, the infiltration of metal melt into the porous preform results in a dense microstructure of the component. Net-shape manufacturing is possible by controlling dimensional changes associated with a displacive reaction between the infiltrated melt and ceramic preform phase. When granules are used as the printing powder, the size of granules decides the thickness of each layer and thus the pore radius of the inter-agglomerate, and the particle size distribution decides the pore radius of the intra-agglomerate. The comparison of a TiC/TiO_2 preform and a TiC preform is summarized in Table 2. The pore size distribution of the two preforms is different, because in the TiC/TiO_2 preform the smaller TiO_2 particles fill the spaces between the large TiC particles and reduce the intra-agglomerate pores fractions.

Table 2: Comparison of the 3DP process of TiC/TiO_2 preform and the TiC preform [10, 37–40].
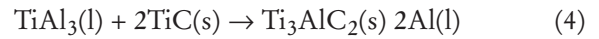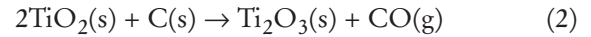
	TiC/ TiO_2 preform	TiC preform
Starting materials	TiC(1.2 μm): TiO_2(30 nm) = 63:31 (weight ratio)	TiC (1.5 μm)
Binder	Dextrin (6 wt%)	Dextrin (10 wt%)
Blending and granulation	Freeze-drying after ball milling	Freeze-drying after ball milling
Printing powder size/shape	~ 200 μm diameter/spherical	~ 200 μm diameter/spherical
Porosity of the green part	55 vol%	—
Density of the sintered part	1.61 g/cm³	1.58 g/cm³
Pore volume fraction	51 vol% (inter), 14 vol% (intra)	38 vol% (inter), 28 vol% (intra)

Post-processing of the preform was conducted in flowing N_2 at 800 °C for 2 h, and it was then sintered in flowing Ar at 1400 °C for 0.5 h. The dextrin decomposed into amorphous carbon in the pre-sintered preform. The bending strength of the 3D-printed preform was lower than 5 MPa, and increased to 5 ~ 10 MPa after pre-sintering [37]. The porosity of the preform increased owing to the pyrolysis of the dextrin during post-processing.

III. Reaction Mechanism

(1) Formation mechanism of Ti_3AlC_2 during RMI

According to Fan *et al.* [56], TiC and Al are thermally stable in the metal melt infiltration temperature range, so an indirect reaction path was designed accordingly. The preform was composed of TiC, TiO_2, and dextrin with a weight ratio of 63:31:6.
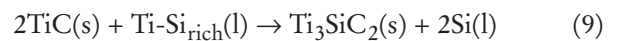
$$2TiO_2(s) + C(s) \rightarrow Ti_2O_3(s) + CO(g) \quad (2)$$

$$Ti_2O_3(s) + 8Al(l) \rightarrow 2TiAl_3(l) + Al_2O_3(s) \quad (3)$$

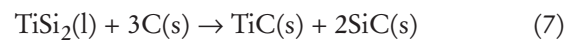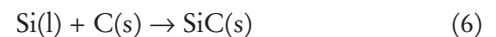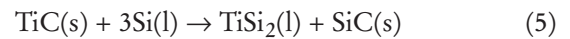$$TiAl_3(l) + 2TiC(s) \rightarrow Ti_3AlC_2(s)\ 2Al(l) \quad (4)$$

The first step of the reaction was the generation of $TiAl_3$. Because the binder material, dextrin, decomposes into amorphous carbon during post-processing, carbon exists in the preform and participates in the reactions. Eq. 3 and Eq. 4 provide a formation path for $TiAl_3$ [57]. The generated Ti_2O_3 during the reaction process was reported to offer better wetting ability with Al melt than TiO_2 at 1400 °C. $TiAl_3$ then reacted with TiC to generate Ti_3AlC_2 [58].

(2) Formation mechanism of Ti_3SiC_2 during RMI

Fan et al. [56] studied the formation mechanism of Ti_3SiC_2 during the RMI process. The study shows that TiC prefers to react directly with Si to form $TiSi_2$ and SiC, the generation of Ti_3SiC_2 requires the formation of TiC twins [59]. The carbon existing in the system reacts with $TiSi_2$ to form new TiC grains rich in carbon vacancies, which promotes the formation of Ti_3SiC_2 owing to the low twin boundary.

The total reaction process could be described as follows: with the infiltration of silicon melt into the preform, silicon melt reacts directly with TiC and carbon particles to form $TiSi_2$ and SiC; with the appearance of $TiSi_2$, Ti-Si_{rich} eutectic is formed as a result of the dissolution of $TiSi_2$ into the silicon melt; TiC particles react with Ti-Si_{rich} eutectic to form Ti_3SiC_2 with the existence of carbon. Eqs. 5 ~ 9 give the reactions that occur during RMI [56, 60].

$$TiC(s) + 3Si(l) \rightarrow TiSi_2(l) + SiC(s) \quad (5)$$

$$Si(l) + C(s) \rightarrow SiC(s) \quad (6)$$

$$TiSi_2(l) + 3C(s) \rightarrow TiC(s) + 2SiC(s) \quad (7)$$

$$Si(l) + TiSi_2(l) \rightarrow Ti\text{-}Si_{rich}(l) \quad (8)$$

$$2TiC(s) + Ti\text{-}Si_{rich}(l) \rightarrow Ti_3SiC_2(s) + 2Si(l) \quad (9)$$

IV. Near-Net-Shape Fabrication during RMI

RMI is a reaction-infiltration competition process, the control between the reaction speed and the infiltration speed is an essential factor for the realization of near-net-shape fabrication. Nan *et al.* printed TiC preforms with a bimodal pore structure by means of 3DP, and the preforms were then infiltrated with liquid silicon at 1600 ~ 1700 °C, to obtain Ti_3SiC_2-based ceramics with favorable mechanical properties and high conductivity [39]. However, a strong volume shrinkage of 51.6 vol% was observed. Subsequently, Al was then introduced into the infiltration melt[40], leading to a decrease in the infiltration temperature. The results showed that the volume shrinkage ratio of samples decreased to 6.43 % and 1.17 % with the

$Al_{40}Si_{60}$ and $Al_{70}Si_{30}$ as the infiltration metal melt, respectively. A similar study was also conducted by Wang *et al.* [61] porous TiC preforms were firstly prepared by means of cold pressing, and then Al-Si alloy infiltration was used to fabricate $Ti_3Si(Al)C_2$-based ceramic, no apparent volume change occurred during the fabrication process. The study also showed that the existence of Al could promote the nucleation of Ti_3SiC_2, because it helps reduce the twin boundary energy of TiC [62].

In contrast, a joint process of three-dimensional printing and reactive melt infiltration realized near-net shape fabrication of a Ti_3AlC_2-based ceramic gearwheel with complex shapes. Fig. 3 shows the CAD model of a gearwheel (left) and the corresponding printed part after RMI. Compared with the pre-sintered preform, the as-fabricated ceramic shows an expansion of 4 % along the in-plane direction and shrinkage of 3.2 % along the out-of-plane direction. The total dimensional change is significantly small compared with the sintering of a powder component, which facilitates the fabrication of bulk materials with complex shape [38].
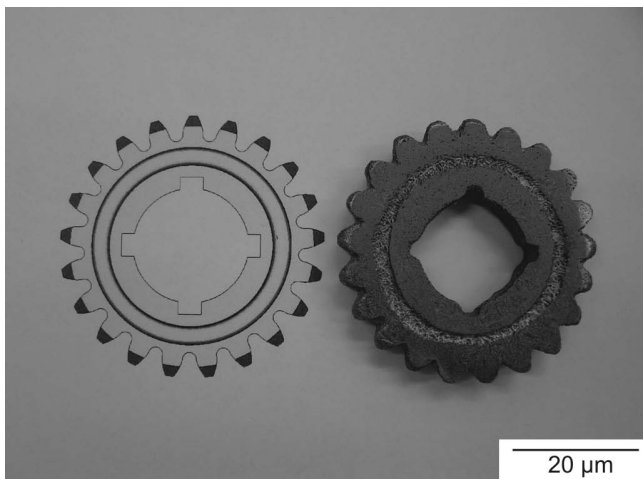

$20 \, \mu m$

Fig. 3 : The CAD model of a gearwheel (left) and the corresponding printed part after RMI [38].

RMI is a reaction-infiltration competition process. For reactive infiltration to be successful, the infiltration rate of the melt into the porous preform should be faster than the reaction rate in order to avoid pore clogging by the reaction product near the surface and incomplete filling of the preform. As the reaction between the molten metal and the porous ceramic preform proceeds, a continuous layer of the reaction product is formed at the melt/preform interface. As a result, the channels through which the molten metal can travel become narrow, thereby reducing the flow. If the reaction kinetics is fast and pores are very fine, complete pore closure and flow cessation may occur (pore clogging). During LSI, the reaction speed stays high and a large amount of solid resultant, for example SiC which has low wettability with Si melt, is generated and cloaks the TiC particles, preventing further infiltration of Si melt into the preform. The insufficient reactant caused the huge volume shrinkage, which could be proved based on the residual TiC in the as-fabricated ceramics. However, the introduction of Al in the infiltration

system significantly reduced the reaction speed in the following discussed ways. Al does not react with TiC and act as a dissolvent, so that the infiltration of Al-Si alloy becomes a controllable process of reaction-dissipation competition. Firstly, the introduction of Al effectively reduces the infiltration temperature, leading to the lower reaction speed. Secondly, the reaction speed decreases further owing to the dilution effect caused by the participation of the Al melt, the concentration of Si is diluted by the participation of Al, and the speed of reaction decreases. Thirdly, the consumed Si during the reaction can only be supplemented through dissipation in the Al melt or Ti-Si-Al melt, in which case the reaction speed of Si is controlled by the dissipation speed. The residual TiC in the as-fabricated material indicates the deficiency of Si during the reaction, which proves the hypothesis of dissipation control during RMI.

V. Microstructure and Mechanical Properties of MAX-Phase-Toughened Ceramics Fabricated with RMI

The phase composition of ceramics fabricated by means of RMI includes intermediate products like $TiAl_3$ or $TiSi_2$, ceramic particles like Al_2O_3 or SiC and some unreacted TiC and residual melt. Since the mechanical properties of different components vary significantly, the effect of phase distribution on the mechanical properties of as-synthesized ceramic parts is significant.

Figs. 4a and b present the typical microstructure of Ti_3SiC_2-and Ti_3AlC_2-based ceramics fabricated with RMI. The bright particles in Fig. 4a are Ti_3SiC_2, the dark areas are $TiSi_2$, TiC particles could be found embedded in both areas. The phase content of Ti_3SiC_2, $TiSi_2$ and TiC are 45, 25 and 21 % respectively. In Fig. 4b the phase with bright contrast is Ti_3AlC_2, the gray phases are $TiAl_3$, the round dark particles are Al_2O_3, the matrix with dark contrast is Al, and the small particles with white contrast are TiC. According to image analysis of the SEM micrographs, the fractions of Ti_3AlC_2, $TiAl_3$, Al_2O_3, Al, and TiC are approximately 35, 30, 10, 20, and 5 vol%, respectively.

Compared with conventional ceramics, MAX phases are damage-tolerant ceramics owing to their special atom bonding and laminated structure. In the loading process, deformation modes of delamination, laminate fracture, buckling and kink-band occur to promote crack deflection, which absorbs lots of energy and favors the improvement of flexural strength and fracture toughness. As shown in Table 3, the Ti_3AlC_2-toughened composites attained a four-point bending strength of 320 ± 40 MPa, and a Young's modulus of 184 ± 24 GPa. The fracture toughness of the as-fabricated sample at 1300 °C is 8.1 ± 1.7 MPa·$m^{1/2}$, the sample fabricated at 1400 °C has an increased K_{IC} of 9.7 ± 0.8 MPa·$m^{1/2}$. The composite with the highest amount (45 vol%) of Ti_3SiC_2 obtained by means of LSI attained a bending strength of 293 ± 17.8 MPa. The composite fabricated with $Al_{70}Si_{30}$ alloy infiltration attained a bending strength of 233 ± 53 MPa and a K_{IC} of 4.6 ± 1.08 MPa·$m^{1/2}$, while the composite obtained with $Al_{40}Si_{60}$ alloy infiltration attained a bending strength of 107 ± 4 MPa and a K_{IC} of 5.9 ± 0.6 MPa·$m^{1/2}$.
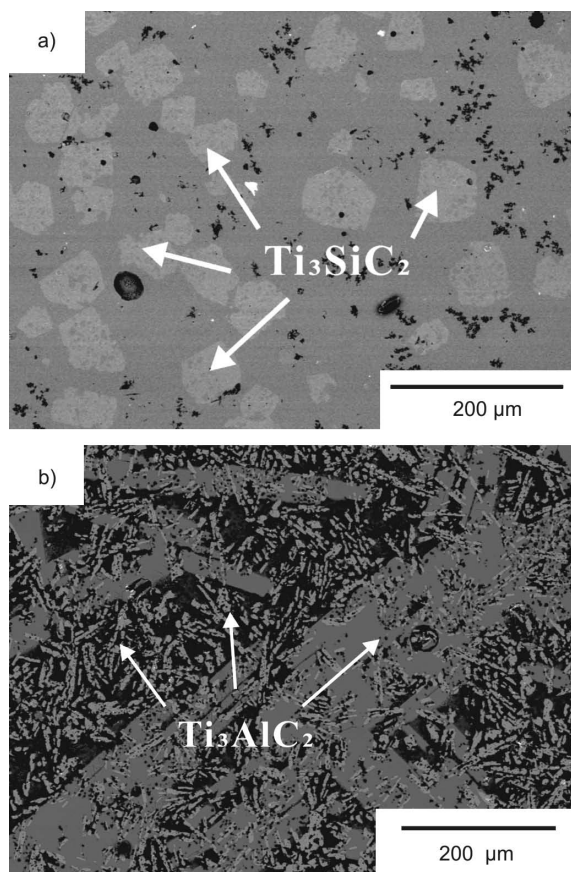
Fig 4: BSE of Ti_3SiC_2 (a)- and Ti_3AlC_2 (b)-based ceramics fabricated with RMI [40, 10].

According to Table 3, the differences in the mechanical properties of the materials are due to the different phase distribution of materials leading to varied properties. Table 4 presents the basic properties of the components in

the as-fabricated ceramics. As can be seen from Table 4, the main phase (Ti_3SiC_2 and Ti_3AlC_2), and the intermediate phase ($TiSi_2$ and $TiAl_3$) of the two ceramics exhibit similar properties. The different mechanical properties of different ceramics can be attributed to to the different phase distribution. Ti_3AlC_2 consists of small rod-shaped grains with small grain size, exhibiting dispersive distribution in the ceramics. These crosslink with each other in the matrix, providing high toughening efficiency. The microstructure-crack path interaction in Ti_3AlC_2-based ceramics is significantly tortuous (Fig. 5), and crack deflection occurs along the weak interface, leading to a fluctuating crack propagation path, which greatly extends the effective crack length and absorbs more fracture energy, leading to an improvement in fracture resistance. However, Ti_3SiC_2 with large particle size is concentrated in specific areas, thus restricting the toughening areas, and between the Ti_3SiC_2 particles are the brittle $TiSi_2$ phase and small TiC particles [38, 40].
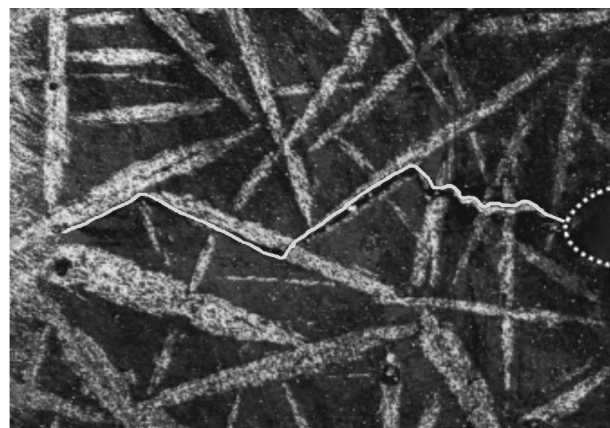

Fig. 5: Optical track micrograph of crack propagation of Ti_3AlC_2 based ceramics fabricated at 1400 °C [38].

Table 3: Bending strength and fracture toughness of different ceramics [38, 39].

	Ti_3AlC_2		Ti_3SiC_2		
	1300 °C	1400 °C	Si	$Al_{40}Si_{60}$	$Al_{70}Si_{30}$
σ_f (MPa)	320±40	—	293±17.8	107±4	233±53
K_{1C}(MPa $\cdot$ m$^{1/2}$)	8.1±1.7	9.7±0.8	—	5.9±0.6	4.6±1.08

Table 4: Basic properties of the components in the as-fabricated ceramics [2, 10, 24, 37 – 39].

Properties	T_M (°C)	ϱ (g/cm^3)	E (GPa)	CTE (×10^{-6}/K)	K_{1C} (MPa $\cdot$ m$^{1/2}$)	σ_f (MPa)	HV (GPa)
Ti_3AlC_2	1400 (decompose)	4.25	297	9	7.2, 4.6	375, 172	3.5
Ti_3SiC_2	1800 (decompose)	4.53	322	8.6, 9.7	8~16	439	4.0
$TiAl_3$	1350	3.37	216	13	2	162	6
$TiSi_2$	1540	4.04	250	9	2~3	170	
Al_2O_3	2015	3.97	380	8.6	3.3	350	16
SiC	2827	3.2	418	4.02	3.5	460	9.2

VI. Conclusions

MAX phases are promising reinforcements for interpenetrating phase composites. RMI is a promising method for the near-net shape manufacturing of MAX-phase-reinforced composites. During the fabrication process, both raw material and pore distribution of the preform should be pre-designed to facilitate the infiltration of metal melt, in order to control deformation as well as the phase distribution of the final material. The control of the reaction speed is an important factor during the fabrication process for control of the deformation. More studies on control of the reaction speed and the reduction of residual alloys should be conducted.

References

[1] Barsoum, M.W., Radovic, M.: Mechanical properties of the MAX phases in encyclopedia of materials science and technology, Elsevier, Amsterdam, (2004).

[2] Barsoum, M.W., El-Raghy, T.: Synthesis and characterization of a remarkable ceramic: Ti_3SiC_2, *J. Am. Ceram. Soc.*, **79**, 1953 – 1956, (1996).

[3] Zhou, Y., Sun, Z., Chen, S., Zhang, Y.: *In-situ* hot-pressing solid-liquid reaction synthesis of dense titanium silicon carbide bulk ceramics, *Mater. Res. Innov.*, **2**, 142 – 146, (1998).

[4] Barsoum, M.W.: The $M_{N+1}AX_N$ Phases: A new class of Solids; thermodynamically stable nano laminates, *Prog. Solid State Ch.*, **28**, 201 – 281, (2000).

[5] Radhakrishnan, R., Henager, C.H., Brimball, J.L., Bhaduri, S.B.: Synthesis of Ti_3SiC_2/SiC and $TiSi_2$/SiC composites using displacement reactions in the Ti–Si–C system, *Scripta. Mater.*, **34**, 1809 – 1814, (1996).

[6] Fan, X., Yin, X., He. S., Zhang, L., Cheng, A.: Friction and wear behaviors of C/C-SiC composites containing Ti_3SiC_2, *Wear*, **27**, 274 – 275, (2012).

[7] Zhang, H., Wang, X., Nickel, K.G., Zhou, Y.: Experimental and thermodynamic study of the hydrothermal oxidation behavior of Ti_3SiC_2 powders, *Scripta. Mater.*, **59**, 746 – 749, (2008).

[8] Yin, X., He, S., Zhang, L., Fan, A., Cheng, L., Tian, G., Li, T.: Fabrication and characterization of a carbon fiber reinforced carbon-silicon carbide-titanium silicon carbide hybrid matrix composite, *Mater. Sci. Eng. A*, **527**, 835 – 841, (2010).

[9] Fan, X., Yin, X.: Microstructure and properties of carbon fiber reinforced SiC matrix composites containing Ti_3SiC_2, *Adv. Eng. Mater.*, **16**, 670 – 683, (2014).

[10] Yin, X., Travitzky, N., Greil, P.: Reactive infiltration processing of Ti_3AlC_2 and Ti_3SiC_2-based composites, Nova Science Publishers, New York Inc. (2012).

[11] Goto, T., Hirai, T.: Chemically vapor deposited Ti_3SiC_2, *Mater. Res. Bull.*, **22**, 1195 – 1202, (1987).

[12] Jacques, S., Fakih, H., Viala, J.C.: Reactive chemical vapor deposition of Ti_3SiC_2 with and without pressure pulses: effect on the ternary carbide texture, *Thin Solid Films*, **518**, 5071 – 5077, (2010)

[13] ³ Yang, C., Jin, S.Z., Liang, B.Y., Jia, S.S.: Low-temperature synthesis of high-purity Ti_3AlC_2 by MA-SPS technique, *J. Eur. Ceram. Soc.*, **29**, 181 – 185, (2009).

[14] Li, S., Zhai, H.: Synthesis and reaction mechanism of Ti_3SiC_2 by mechanical alloying of elemental Ti, Si, and C powders, *J. Am. Ceram. Soc.*, **88**, 2092 – 2098, (2005).

[15] Gauthier, V., Cochepin, B., Dubois, S.: Self-propagating high-temperature synthesis of Ti_3SiC_2: Study of the reaction mechanisms by time-resolved X-ray diffraction and infrared thermography, *J. Am. Ceram. Soc.*, **89**, 2899 – 2907, (2006).

[16] Meng, F., Liang, B., Wang, M.: Investigation of formation mechanism of Ti_3SiC_2 by self-propagating high-temperature synthesis, *Int. J. Refract. Met. H.* **41**, 152 – 161, (2013).

[17] Yeh, C.L., Shen, Y.G.: Effects of using Al_4C_3 as a reactant on formation of Ti_3AlC_2 by combustion synthesis in SHS mode, *J. Alloy. Compd.*, **473**, 408 – 413, (2009).

[18] Li, S., Song, G., Zhou, Y.: Dense and fine-grained SiC/$Ti_3Si(Al)C_2$ composite and its high-temperature oxidation behavior, *J. Eur. Ceram. Soc.*, **32**, 3435 – 3444, (2012).

[19] Tzenov, N.V., Barsoum, M.W.: Synthesis and characterization of Ti_3AlC_2, *J. Am. Ceram. Soc.*, **83**, 825 – 832, (2000)

[20] Han, J.H., Hwang, S.S., Lee, D., Park S.W.: Synthesis and mechanical properties of Ti_3AlC_2 by hot pressing TiC_x/Al powder mixture, *J. Eur. Ceram. Soc.*, **28**, 979 – 988, (2008).

[21] Gao, N.F., Li, J.T., Zhang, D.: Rapid synthesis of dense Ti_3SiC_2 by spark plasma sintering, *J. Eur. Ceram. Soc.*, **22**, 2365 – 2370, (2002).

[22] Zhou, Y., Zhang, H., Liu, M.: Preparation of TiC free Ti_3SiC_2 with improved oxidation resistance by substitution of si with al, *Mater. Res. Innov.*, **8**, 97 – 102, (2004).

[23] Arunajatesan, S., Carim, A.H.: Synthesis of titanium silicon carbide, *J. Am. Ceram. Soc.*, **78**, 667 – 672, (1995).

[24] Sun, W., Dcosta, D., Lin, F., El-Raghy, T.: Freeform fabrication of Ti_3SiC_2 Powder-based structures part I-integrated fabrication process, *J. Mater. Proc. Technol.*, **127**, 343 – 351, (2002).

[25] Sachs, E., Cima, M., Williams, D., Brancazio, D., Cornie, J.: Three dimensional printing rapid tooling and prototypes directly from a CAD model, *CIRP Ann. Manuf. Techn.*, **39**, 201 – 204, (1990).

[26] Sachs, E., Cima, M., Williams, D., Brancazio, D., Cornie, J.: Three dimensional printing rapid tooling and prototypes directly from a CAD model, *J. Manuf. Sci. Eng.*, **114**, 481 – 488, (1992).

[27] Chua, C.K., Leong, K.F., Lim, C.S.: Rapid prototyping: principles and applications, 3rd edition. World Scientific, Singapore, 2010.

[28] Song, J.H., Edirisinghe, M.J., Evans, J.R.G.: Formulation and multilayer jet printing of ceramic inks, *J. Am. Ceram. Soc.*, **82**, 3374 – 3380, (1999).

[29] Sachs, E., Cima, M., Bredt, J., Curodeau, A., Fan, T., Brancazio, D.: CAD-casting: Direct fabrication of ceramic shells and cores by three-dimensional printing, *Manuf. Rev.*, **5**, 117 – 126, (1992).

[30] Lejeune, M., Chartier, T., Dossou-Yovo, C., Noguera, R., Inkjet printing of ceramic micro-pillar arrays, *J. Eur. Ceram. Soc.*, **29**, 905 – 911, (2009).

[31] Greil, P.: Biomorphous ceramics from lignocellulosics, *J. Eur. Ceram. Soc.*, **21**, 105 – 118, (2001).

[32] Greil, P.: Near net shape manufacturing of ceramic, *Mater. Chem. Phys.*, **61**, 64 – 68, (1999).

[33] Windsheimer, H., Travitzky, N., Hofenauer, A., Greil, P.: Laminated object manufacturing of preceramic-paper-derived SiSiC composites, *Adv. Mater.*, **19**, 4515 – 4519, (2007).

[34] Moon, J., Caballero, A.C.: Fabrication of functionally graded reaction infiltrated SiC-si composite by three-dimensional printing (3DP) process, *Mater. Sci. Eng. A*, **298**, 110 – 119, (2001).

[35] Travitzky, N., Zimmermann, K., Melcher, R., Greil, P.: From polysaccharides to SiSiC composites by 3D printing, *Ceram. Trans.*, **175**, 37 – 45, (2006).

[36] Fu, Z., Schlier, L., Travitzky, N., Greil, P.: Three-dimensional printing of SiSiC lattice truss structures, *Mater. Sci. Eng. A,*, **560**, 851 – 856, (2013).

[37] Yin, X., Travitzky, N., Greil, P.: Near-net-shape fabrication of Ti_3AlC_2-based composites, *Int. J. Appl. Ceram. Technol.*, **4**, 184 – 190, (2007).

38 Yin, X., Travitzky, N., Greil, P.: Three-dimensional printing of nanolaminated Ti_3AlC_2 toughened $TiAl_3$–Al_2O_3 composites, *J. Am. Ceram. Soc.*, **90**, 2128 – 2134, (2007).

39 Nan, B., Yin, X., Zhang, L., Cheng, L.: Three-dimensional printing of Ti_3SiC_2-based ceramics, *J. Am. Ceram. Soc.*, **94**, 969 – 972, (2011).

40 Ma, Y., Yin, X., Fan, X., Wang, L., Greil, P., Travitzky. N.: Near-Net-shape fabrication of Ti_3SiC_2-based ceramics by three-dimensional printing, *Int. J. Appl. Ceram. Technol.*, **12**, 71 – 80, (2015).

41 Voytovych, R., Bougiouri, V., Calderon, N.R., Narciso, J., Eustathopoulos, N.: Reactive infiltration of porous graphite by NiSi alloys, *Acta Mater.*, **56**, 2237 – 2246, (2008).

42 Fan, X., Yin, X., Wang, L., Zhang, L., Cheng, L.: Processing, microstructure and ablation behavior of C/SiC-Ti_3SiC_2 composites fabricated by liquid silicon infiltration, *Corros. Sci.*, **74**, 98 – 05, (2013).

43 Wan, D., Zhou, Y., Hu, C., Bao, Y.: Improved strength-impairing contact damage resistance of $Ti_3Si(Al)C_2$/SiC composites, *J. Eur. Ceram. Soc.*, **27**, 2069 – 2076, (2007).

44 Lu, C., Yin, X., Li, X.: A Novel *in-situ* synthesis route of Ti_3SiC_2-SiC Composite by Liquid Silicon Infiltration, *J. Inorg. Mater.*, **25**, 1003 – 1008, (2010).

45 Shan, D., Yan, G., Zhou, L., Li, C., Li, J., Liu, G., Feng, J.: Synthesis of Ti_3SiC_2 bulks by infiltration method, *J. Alloy. Compd.*, **509**, 3602 – 3605, (2011).

46 Hwang, S., Han, J., Lee, D., Park, S.: Synthesis of Ti_3SiC_2 by infiltration of molten si, *J. Alloy. Compd.*, **509**, 336 – 339, (2011).

47 Kang, Y., Fey, T., Greil, P.: Synthesis of Ti_2SnC MAX phase by mechanical activation and melt infiltration, *Adv. Eng. Mater.*, **14**, 85 – 91, (2012).

48 Lenz, F., Krenkel, W.: Carbon fiber reinforced ceramics based on reactive melt infiltration processes, *J. Korean Ceram. Soc.*, **49**, 287 – 294, (2012).

49 Messner, R.P., Chiang, Y.M.: Liquid-phase reaction-bonding of silicon carbide using alloyed silicon–molybdenum melts, *J. Am. Ceram. Soc.*, **73**, 1193 – 1200, (1990).

50 Travitzky, N., Bonet, A., Dermeik, B., Fey, T., Filber-Demut, I., Schlier, L., Schlordt, T., Greil, P.: Additive manufacturing of ceramic-based materials, *Adv. Eng. Mater.*, **16**, 729 – 754, (2014).

51 Leukers, B., Gulkan, H., Irsen, S.H., Milz, S., Tille, C., Schieker, M.: Hydroxyapatite scaffolds for bone tissue engineering made by 3D printing, *J. Mater. Sci. Mater. Med.*, **16**, 1121 – 1124, (2005).

52 Utela, B., Storti, D., Anderson, R., Ganter, M.: A review of process development steps for new material systems in three dimensional printing (3DP), *J. Manuf. Process.*, **10**, 96 – 104, (2008).

53 Sachs, E.M., Cima, M.J., Caradonna, M.A.: Jetting layers of powder and the formation of fine powder beds thereby, U.S. Patent and Trademark Office, Massachusetts Institute of Technology, 6, 596, 224, (2003).

54 Fierz, F.C., Beckmann, F., Huser, M., Irsen, S.H., Leukers, B., Witte, F., Degistirici, Ö., Andronache, A., Thie, M., Müller, B.: The morphology of anisotropic 3D-printed hydroxyapatite scaffolds, *Biomaterials*, **29**, 3799 – 3806, (2008).

55 Butscher, A., Bohner, M., Roth, C. Ernstberger, A., Heuberger, C., Doebelin, N., Rohr, P.R.V., Müller, R.: Printability of calcium phosphate powders for three-dimensional printing of tissue engineering scaffolds, *Acta Biomater.*, **8**, 373 – 385, (2012).

56 Fan, X., Yin, X., Wang, L., Greil, P., Travitzky, N.: Synthesis of Ti_3SiC_2-based materials by reactive melt infiltration, *Int. J. Refract. Met. H.*, **45**, 1 – 7, (2014).

57 Wagner, F., Garcia, D.E., Krupp, A., Claussen, N.: Interpenetrating Al_2O_3-$TiAl_3$ alloys produced by reactive infiltration, *J. Eur. Ceram. Soc.*, **19**, 2449 – 2453, (1999).

58 Chen, J., Li, J., Zhou, Y.: *In-situ* synthesis of Ti_3AlC_2/TiC-Al_2O_3 composites from TiO_2-Al-C system, *J. Mater. Sci. Tech.*, **22**, 455 – 458, (2006).

59 Yu, R., Zhan, Q., He, L., Zhou, Y., Ye, H.: Si-induced twinning of TiC and formation of Ti_3SiC_2 platelets, *Acta. Mater.*, **50**, 4127 – 4135, (2002).

60 Lina, Z., Zhuo, M., Zhou, Y., Li, M., Wang, J.: Microstructural relationships between compounds in the ti-si-C system, *Scripta Mater.*, **55**, 445 – 448, (2006).

61 Wang, L., Yin, X., Fan, X., Greil, P., Travitzky, N.: $Ti_3Si(Al)C_2$-based ceramics fabricated by reactive melt infiltration with $Al_{70}Si_{30}$ alloy, *J. Eur. Ceram. Soc.*, **34**, 1493 – 1499, (2014).

62 Yu, R., He, L., Ye, H., Effects of Si and Al on twin boundary energy of TiC, *Acta Mater.*, **51**, 2477 – 2484, (2003).